

Ultra-Low Velocity Zones Near the Core-Mantle Boundary from Broadband PKP Precursors

Lianxing Wen* and Donald V. Helmberger

Short- and long-period precursors of the PKP phase were used to study an ultra-low velocity zone (ULVZ) near the core-mantle boundary beneath the Western Pacific. Synthetic seismograms were computed from a hybrid method, which handles seismic wave propagation through two-dimensional complex structures. Long-period precursors were explained by Gaussian-shaped ULVZs of 60 to 80 kilometers height with P velocity drops of at least 7 percent over 100 to 300 kilometers. Short-period precursors suggest the presence of smaller scale anomalies accompanying these larger Gaussian-shaped structures. These fine structures may be areas of partial melt caused by vigorous small-scale convection or the instability of a thermal boundary layer at the mantle's base, or both.

The scale, magnitude, and geometry of seismic heterogeneities near the core-mantle boundary (CMB) region help define the mineralogy (1, 2) and the geodynamic (3, 4) evolution of Earth. Whereas global seismic tomography has revealed large-scale seismic structure of a slower than average mid-Pacific surrounded by a doughnut-shaped faster than average circum-Pacific region with velocity perturbations of up to 3% in the lower mantle (5), recent studies of core phases suggest the existence of ULVZs beneath Iceland (6) and the western Pacific regions (7–10). The western Pacific region appears to be unique in that the deep seismicity associated with the Tonga-Fiji seismic zone produces high-quality seismograms recorded globally. Figure 1 shows the sampled CMB regions in the western Pacific from previous studies, along with seismic velocity perturbations in the lowermost mantle (11). Unfortunately, the detailed structures of these ULVZs are poorly constrained [see, for example, (9)].

Although short PKP precursors have been noted on the worldwide standard seismic network (WWSSN) for many years (12), they have not been used in combination with long-period precursors. Long-period energy arriving before PKP was noted (13); however, these signals were attributed to PKP diffractions unrelated to CMB structures. We observed long- and short-period precursors of PKP at stations from Eastern Europe to Iran for earthquakes that occurred in the Fiji subduction zone (see Fig. 2 for examples of the long-period PKP precursors). With these observations and recent development of techniques for calculating synthetic seismograms (9), we were able to

map detailed localized seismic structures in the CMB region that satisfy the long- and short-period data. We present results for one event (Table 1, event 1). The PKP ray paths to two representative stations (TAB and UME) of the Fiji event are labeled "A" and "B" in Fig. 1. The heavy lines in Fig. 1 indicate the source-side core-mantle boundary regions sampled by

the precursors. Seismograms recorded by long- and short-period WWSSN instruments at stations TAB and UME are shown (Fig. 3, A and B).

The short-period records (Fig. 3) show a distribution of strong precursors to the geometric PKP arrivals, similar to the observation of Vidale and Hedlin (10). Similar results are seen at other stations with different degrees of complexity. Some long-period phases arriving before the PKP phases in synthetic seismograms of one-dimensional (1D) models, such as PREM (Preliminary Earth Reference Model) (14), are essentially caused by diffraction of the rays into the fluid-core shadow zone, but they are very long period in character, as shown by the synthetics labeled PREM (Fig. 3, A and B) (15, 16). These long-period observations show clear arrivals with periods similar to PKP.

At epicentral distances (120° to 144°), the first arrival is PKP (PKIKP or PKPdf) (Fig. 4). For a radially symmetric Earth model such as PREM, there is no geometric arrival possible through the outer core because of the shadow zone resulting from the P wave velocity drop from the mantle

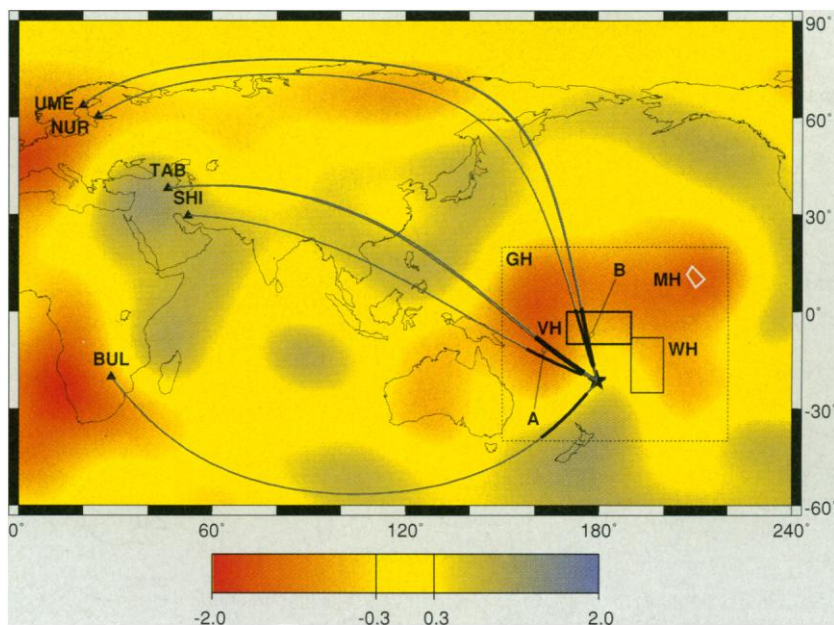


Fig. 1. The sampled CMB regions in the Western Pacific from previous studies, along with the large-scale seismic velocity structure of Su *et al.* (11) of the lowermost mantle. The dashed box GH contains results of Garnero and Helmberger (7) on the ultra-low velocity layers with P velocity reduction of up to 10% from long-period SKS (SV wave in the mantle and P wave in the fluid core) and SPdKS (containing a P -diffracted segment along the CMB); the solid box WH reports on modeling a 2D structure 40 km high with a P velocity drop of 10% and an S velocity drop of 30%, and a horizontal length scale of 250 km from long-period SKS and SPdKS phases (9); the white box MH reports on strong P velocity reductions to explain the precursors to short-period PcP (reflected wave from the CMB) by Mori and Helmberger (8); and the heavy lined box (left of box WH) is reported to contain strong scatterers that explain intense short-period precursors to PKP phase, which are observed at NORSAR, a seismic station array near UME (10). The labeled shaded lines (A and B) are the CMB regions sampled by the PKP precursors at stations TAB and UME studied here. The locations of three events (Table 1) are represented by the stars (three stars are essentially superimposed). The 2D structures (A and B) are shown in Fig. 6.

Seismological Laboratory, California Institute of Technology, Pasadena, CA 91125, USA.

*To whom correspondence should be addressed. E-mail: wen@gps.caltech.edu

to the core. However, if there are scatterers (seismic anomalies) in the lowermost mantle, seismic rays effectively change their ray parameter and propagate back to Earth's surface by other paths through the outer core. Some of those perturbed rays can arrive earlier than the PKP phase and appear as precursors to PKP (Fig. 4) (12, 17, 18). The arrival time of the precursor depends on the radial and lateral location of the scatterer, and the amplitude of the precursor constrains the size and geometry of the scatterer. Thus, the timing and amplitude of precursors, especially broadband observations, provide a unique opportunity to explore the scale, magnitude, and geometry of fine seismic structures in the lowermost mantle. Figure 5 shows the relative travel time of precursors to PKP phase as a function of lateral distance of

the corresponding scatterers, assuming four different depths of the scattering. Each trace corresponds to an event-receiver pair at a certain distance. It is obvious that, for some distance ranges, there is a trade-off between the depth and lateral location of possible scatterers for a precursor arriving in a certain time window, and furthermore, scatterers beneath receivers can cause scattering as well.

Several independent lines of evidence suggest that the broadband PKP precursors in Fig. 3, A and B, are caused by source-side scattering: (i) Source-side regions appear to have slower than average velocity in global seismic tomographic models (11); (ii) the adjacent regions on the source side appear to be very anomalous (Fig. 1); and (iii) the apparent velocities of PKP precursors of two azimuths (A for TAB and SHI and B for

UME and NUR) are consistent with source-side scattering.

Adopting the value of correlation length (8 km) of scattering obtained from globally averaged data, based on the assumption of uniform scattering (4), at least 8% of a root-mean-square velocity perturbation is required to explain the observed short-period scattered energy (Fig. 3). Although the amplitudes of the short-period precursors are predicted by this random model, the waveforms do not fit the data. Moreover, random models do not produce significant long-period energy precursors. The long-period waveforms from the random model are similar to those produced by PREM. Coherent and continuous larger scale structures are required to explain the long-period precursors.

The earliest arrival of a precursor recorded at TAB is consistent with scatterers located at the lowermost 150 km of the mantle. However, because of the trade-off between depth and lateral location of those scatterers, the exact location of scatterers cannot be determined from UME data alone. We assumed that the scatterers were located at the bottom of the mantle, to be consistent with the PcP data (8).

Table 1. Fiji events.

Event	Time	Latitude/longitude	Depth (km)	Magnitude
1	12 September 1968	21.6°S, 179.4°W	635	5.9
2	17 March 1966	21.1°S, 179.2°W	627	5.9
3	9 October 1967	21.1°S, 179.2°W	605	6.2

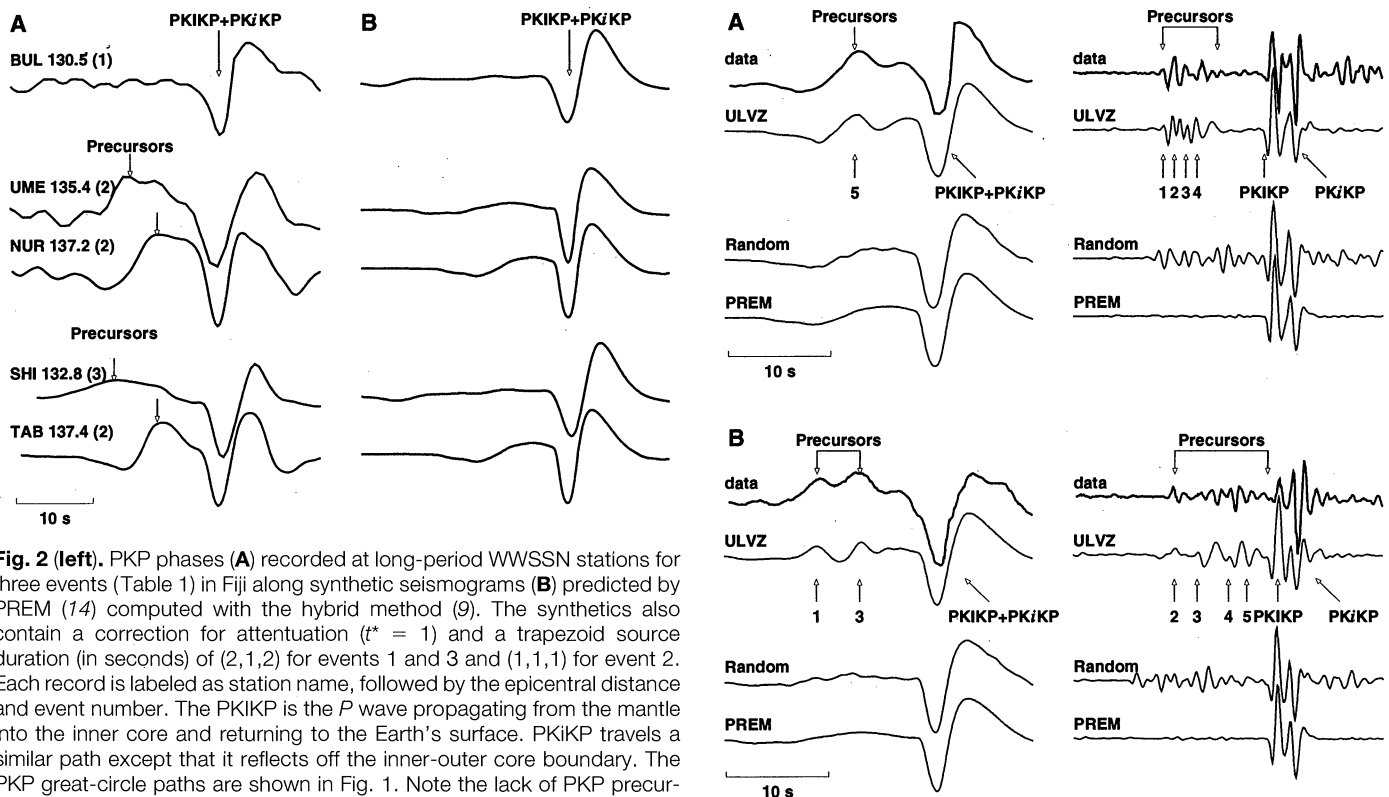
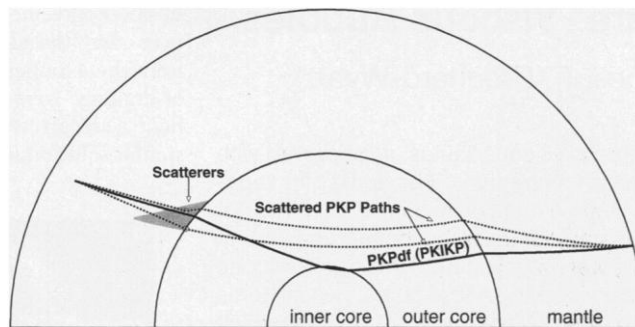


Fig. 2 (left). PKP phases (A) recorded at long-period WWSSN stations for three events (Table 1) in Fiji along synthetic seismograms (B) predicted by PREM (14) computed with the hybrid method (9). The synthetics also contain a correction for attenuation ($t^* = 1$) and a trapezoid source duration (in seconds) of (2,1,2) for events 1 and 3 and (1,1,1) for event 2. Each record is labeled as station name, followed by the epicentral distance and event number. The PKIKP is the P wave propagating from the mantle into the inner core and returning to the Earth's surface. PKJ/KP travels a similar path except that it reflects off the inner-outer core boundary. The PKP great-circle paths are shown in Fig. 1. Note the lack of PKP precursors observed at station BUL. **Fig. 3 (right).** The observed long- and short-period PKP phase and precursors along with synthetics produced by various models at TAB (A) and UME (B). Three sets of synthetics are displayed, based on PREM, a random model (correlation length of 8 km and root-mean-square variation of 8%), and the ultra-low velocity structures shown in Fig. 6. The arrows indicated by the numbers correspond to

the precursors produced by the structures as indexed in Fig. 6. All synthetics are calculated by the hybrid method (9). The smaller observed PKIKP phases compared to synthetics of 1D models have been attributed to the absorption of the uppermost inner core (18, 22). Therefore, the precursors should be compared to PKIKP in assessing their strength.

Fig. 4. A display of ray paths of PKIKP and precursors of PKP at an epicentral distance of 136°. The shaded region indicates the scatterer locations, which will produce seismic arrivals before the PKIKP phase. The reference model is PREM (14).



Numerical tests indicate that structures with horizontal and vertical length scales of 100 to 300 km and 60 to 80 km, respectively, and *P* wave velocity drops of at least 7% are required to explain the observed long-period precursors. The timing of short-period precursors suggests that small-scale structures accompany, rather than be superimposed on, the large-scale structures (Fig. 6). Long- and short-period synthetics produced by these two structures (Fig. 3) fit the data. Although the details of the real structure may be different from our 2D models, the overall structure of our 2D models is representative of the scale, magnitude, and geometry of real structures. Because the behaviors of short-period observation are affected by many factors, we have not made further efforts to modify our 2D models to find a better fit to the short-period precursors.

We tested a number of other possible explanations, such as topographic relief, as

proposed by Doornbos (19). However, topography at the CMB even with a magnitude of 5 km produces little long-period energy. Although the topography at the CMB may contribute some portion of precursor energy, it is unlikely that the topographic effects can explain the data. The long-period precursors are generated by the wide-angle reflection from the right-hand side of the Gaussian-like structures. However, there is a trade-off between the *P* wave velocity decrease and heights of the structures, but structures with *P* wave velocity drops of at least 7% are required to produce synthetics that fit these particular records.

Broadband precursors can be explained by ULVZs with different length scales. A thin (for example, 5 km) ULVZ will produce short-period precursors, as normally observed, if it is sufficiently rough. Structures with these length scales are, however, less detectable from SKS and SKPdKS waveforms (20). It is conceivable that many ULVZs are undetected in the mid-Pacific and other hotter-than-average re-

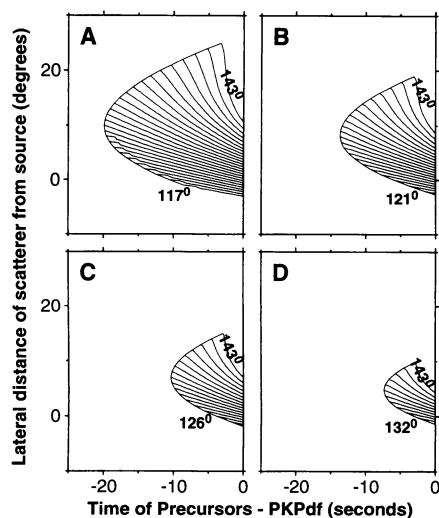


Fig. 5. Plots of travel time of precursors as a function of lateral distance of scatterers from a seismic source. Each panel assumes a different depth of scatterer: (A) the CMB; (B) 200 km above the CMB; (C) 400 km above the CMB; and (D) 800 km above the CMB. Each trace corresponds to an event-receiver pair. The increment of epicentral distance between traces is 1°.

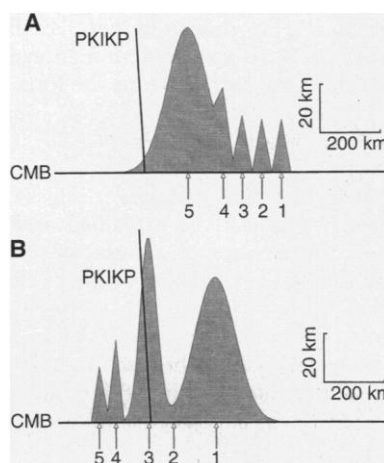


Fig. 6. The 2D cross sections of seismic structure derived by fitting the broadband PKIKP precursors observed at TAB (A) and UME (B). The geographic locations of these 2D cross sections are indicated by heavy lines ("A" and "B") in Fig. 1. The numbers indicate structures which produce precursors as indexed in Fig. 3. The shaded regions have a *P* velocity drop of 10%.

gions, because of their small dimensions and data coverage. PKP precursors are absent from paths that sample beneath the Americas (21, 22), the lowermost mantle of which is faster and presumably colder than the average lowermost mantle (11). The correlation of absence (presence) of ULVZ and weak (strong) PKP precursors suggests that ULVZs with different length scales may be major contributors to broadband PKP precursors.

The magnitudes of *P* wave velocity drops of these ULVZs and the *S* wave velocity drop of 30% of other ULVZs (9) are consistent with partial melt (1). The length scale and geometry of these ULVZs suggest that these ULVZs may be indicative of small-scale mantle convection or instability of the bottom thermal boundary layer of the mantle, or both.

REFERENCES AND NOTES

1. Q. Williams and E. J. Garnero, *Science* **273**, 1528 (1996).
2. K. G. Holland and T. J. Ahrens, *ibid.* **275**, 1623 (1997).
3. P. Olsen, G. Schubert, C. Anderson, *Nature* **327**, 409 (1987).
4. M. A. H. Hedlin, P. M. Shearer, P. S. Earle, *ibid.* **387**, 145 (1997).
5. X.-F. Liu and A. M. Dziewonski, *Eos (Fall Suppl.)* **75** (no. 44), 663 (1994).
6. D. V. Helmberger, L. Wen, X. Ding, *ibid.* **78** (no. 46), F1 (1997).
7. E. J. Garnero and D. V. Helmberger, *Phys. Earth Planet. Inter.* **91**, 161 (1995).
8. J. Mori and D. V. Helmberger, *J. Geophys. Res.* **100**, 20359 (1995).
9. L. Wen and D. V. Helmberger, *ibid.*, in press. The hybrid method is a combination of numerical and analytical methods, with the numerical method (finite-difference) applied in the heterogeneous regions only. This allows a high-resolution study. Generalized ray-theory solutions from a seismic source are used in the finite-difference initiation process, and seismic motions are propagated back to the Earth's surface analytically with the aid of the Kirchhoff method.
10. J. E. Vidale and M. Hedlin, *Nature* **391**, 682 (1998).
11. W. J. Su, R. L. Woodward, A. M. Dziewonski, *J. Geophys. Res.* **99**, 6945 (1994).
12. R. A. Haddon and J. R. Cleary, *Phys. Earth Planet. Inter.* **8**, 211 (1974).
13. G. R. Buchbinder, *Bull. Seismol. Soc. Am.* **64**, 33 (1974).
14. A. Dziewonski and D. L. Anderson, *Phys. Earth Planet. Inter.* **25**, 297 (1981).
15. R. Kind and G. Müller, *J. Geophys.* **41**, 149 (1975).
16. V. F. Cormier and P. G. Richards, *ibid.* **43**, 3 (1977).
17. J. R. Cleary and R. A. W. Haddon, *Nature* **240**, 549 (1972).
18. V. F. Cormier, *Geophys. J. Int.* **121**, 725 (1995).
19. D. J. Doornbos, *Geophys. J. R. Astron. Soc.* **53**, 643 (1978).
20. D. V. Helmberger, E. J. Garnero, X. Ding, *J. Geophys. Res.* **101**, 13963 (1996).
21. K. Bataille, R.-S. Wu, S. M. Flatte, *Pure Appl. Geophys.* **132**, 151 (1990).
22. X. D. Song and D. V. Helmberger, *J. Geophys. Res.* **100**, 9805 (1995).
23. We thank T. Ahrens, D. Anderson, R. Clayton, M. Gurnis, H. Kanamori, T. Melbourne, and D. Stevenson for reviews. Funded by NSF grants EAR-9316441 and EAR-9629279. This paper is Contribution No. 8501, Division of Geological and Planetary Sciences, California Institute of Technology.

27 October 1997; accepted 2 February 1998